Hindawi
Advances in Mathematical Physics
Volume 2019, Article ID 7134309, 12 pages
https://doi.org/10.1155/2019/7134309

Research Article

Analysis and Optimization of a Cyclone Integrated with a Cartridge Filter in a Hazardous Materials Collection Truck

Shuwen Zhou and Yu Wang

College of Mechanical Engineering and Automation, Northeastern University, Shenyang, Liaoning 110819, China

Correspondence should be addressed to Yu Wang; yu.wang1995@tom.com

Received 1 February 2019; Revised 13 March 2019; Accepted 26 March 2019; Published 8 April 2019

Academic Editor: Yannis Dimakopoulos

In order to meet the filtration separation of hazardous materials on hazardous materials collection truck, the most popular separation devices, such as the cyclone separator and the filter cartridge, are combined to form a new filtration device in this study. The advantages of the two devices are utilized to achieve effective separation of solid particles and prevent secondary pollution. Among the various structural influence factors of filtration equipment, four structural parameters that affect the separation performance significantly are selected as optimization variables. The response surface methodology was used to design the simulation experiment. Using fluid mechanics analysis software, multiple sets of parameters were simulated. Then, the simulation data was used to establish a mathematical model of separation efficiency, and structural optimization analysis was performed based on the mathematical model. Finally, the results show that the inner exhaust pipe diameter and the cone height have more influence on the efficiency of the cyclone separation structure. The interaction between the diameter and insertion depth of the inner exhaust pipe is also obvious. Among the four optimization variables, there is an optimum value for the inner exhaust pipe insertion depth, and the effect of the other three factors on the separation efficiency is monotonic. In the case of a total separation efficiency of 99.9% and after optimizing the combined model within a reasonable interval, 81.25% of the 1-μm particles can be removed by the cyclone separation part, and only 18.75% are removed by the filter cartridge.

1. Introduction

Cyclone devices are widely used in heavy industry and light industry, acting as either classifiers or separators. Their applications are extensive, including but not limited to the separation or classification of plastic fines, sand, plastic and metal pellets, rock, and carbon fines [1]. Cyclone separators are commonly used as gas-solid separators (i.e., dedusting) and as gas-liquid separators (i.e., demisting), intended to enable at least partial elimination of solid or liquid particles from the gas stream. The cartridge type dust collector is a separator represented by a filtration separation method, which can effectively capture particles from 0.1um to 5 um. It has the advantages of high efficiency, compact structure, and so on. It is widely used in various industries.

A common cyclone separator can remove dust particles exceeding 5 μm in diameter effectively from a gas stream, but its efficiency will drop dramatically as the dust size decreases. Although a specially designed cyclone can remove smaller particles, it is not economical in industrial applications [1]. A cartridge filter can separate very small diameter particles from the gas stream but needs a large amount of space. In addition, if all particles are removed from the surface of the filter cartridge, then the blockage and breakage of the filter cartridge will increase, resulting in frequent replacement. Therefore, the filter cartridge dust collector maintenance fee will be higher. They cannot achieve good dust removal effect when used alone. Although they can be used in the method of multistage parallel, because of taking up too much area, they are not suitable for this method in the hazardous materials collection truck. If the cyclone can be integrated with the filter cartridge filter, then the combined separator has the characteristics of high separation efficiency, and it can also separate corrosive hazardous materials, making room for other functions of the hazardous materials collection truck, as shown in Figure 1.

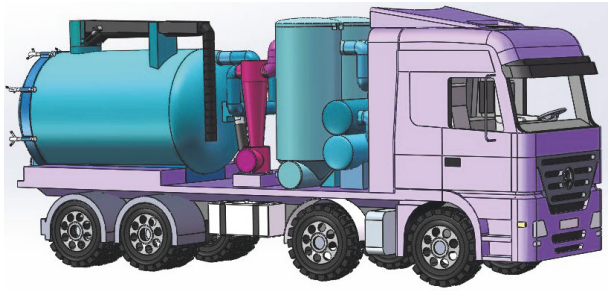

Figure 1: Hazardous materials collection truck.

Separation efficiency and pressure loss are the two most relevant evaluation criteria for cyclone performance. Therefore, it is necessary to establish a reasonable mathematical model to represent the relationship between the cyclone performance and characteristics. There are currently three main methods to describe the cyclone performance: mathematical models (theoretical and semiempirical models) [2–4], statistical models (experimental investigation) [5–7], and computational fluid dynamics models (CFD models) [8–10]. As the theoretical and semiempirical models were derived from physical descriptions and mathematical equations using many assumptions and simplified conditions, different models can lead to significant differences between predicted and measured results [11]. Although statistical models are more convenient for predicting the cyclone pressure drop, it is significantly more difficult to determine the most appropriate correlation function for fitting experimental data [11, 12]. The CFD focuses on the construction and solution of the governing equations and the study of various approximations to these equations. CFD presents the perfect opportunity to study specific terms in the governing equations in a more detailed fashion and complements experimental and analytical approaches by providing an alternative cost-effective means of simulating real fluid flows [13].

An integrated fluid dynamics model of cyclone and cartridge filter has been investigated. The combined separator is simulated and analyzed. The total separation efficiency of the combined model is high owing to the presence of the filter cartridge. Therefore, in this study, the structural parameters of the combined model are optimized to reduce the capture rate of the filter cartridge. This method will reduce the particle packing speed on the surface of the filter cartridge, reducing the frequency of cleaning and increasing the working life of the filter cartridge. Finally, the purpose of the structural optimization was achieved. Given that the separator performance is closely related to the geometry of the combined separator and these geometric parameters are constrained by each other, there are optimal values for these parameters. There are currently two methods that are used in the optimization design of the separator: single-objective optimization [11, 14] and multiobjective optimization [15–17]. Therefore, it is necessary to comprehensively consider the influence of multiple influencing factors and their interaction on the capture efficiency of the lower part of the model. However, there are many combinations of multiple structural parameters within a certain range. Therefore, the experiment was designed using Design-Expert software. Based on the obtained simulation experimental data, a mathematical model used for analysis is established and the optimal value of structure optimization is obtained within a small number of experiments.

2. The Combined Model and Numerical Simulation

2.1. The Analysis of Function and Structure

2.1.1. The Introduction of Filter Cartridge. The filter cartridge is evolved from the filter bag, consisting of a top cover, a metal frame, a seal ring, and a base bracket. Filter cartridge includes inner, outer, and middle layers. The inner and outer layers are composed of wire-netting, and the filter media is repeatedly folded to form a middle layer. The filter cartridge is characterized in that it adheres a layer of submicron ultrathin fibers to the filter media. The fibers on the adhesive layer are arranged very closely, with a gap of 0.12~0.6um. In recent years, with the development of technology and the continuous innovation of new materials, the filter media of the dust collector has been improved in countries represented by the United States and Japan. This article selects Ultra-web new filter media, which is the filter media of filter cartridge type dust collector produced by American Donaldson Company. It has a dust removal efficiency of 99.9% for a particle size of 0.5um [18, 19].

Because the filter cartridges evolved from filter bags, they work similarly. Small particles of hazardous materials will enter the dust chamber with the airflow, and the particles will accumulate on the surface of the filter media through the screening of the filter cartridge. The clean air passes through the filter cartridge and eventually flows out of the outer exhaust pipe. When the particles on the surface of the filter media accumulate to a certain extent and the pressure of the outer exhaust pipe increases to a certain extent, the cleaning device removes the particles on the surface of the filter media. Finally the particles fall into the dust outlet and are captured. The filtration mechanism of filter media mainly includes interception effect, inertial effect, and diffusion effect. Interception effect: the arrangement inside the filter media is intricate and intertwined. The average pore size of the filter media is small, and the particles having a diameter larger than the pore size of the filter media cannot be intercepted through the gap of the filter layer. Inertial effect: when the particles move with the airflow, the airflow encounters obstacles and bypasses, while the dust is collected as the inertia deviates from the direction of the airflow and hits the filter layer [18]. Most of the dust particles will be filtered by a variety of filtration mechanisms.

2.1.2. The Introduction of Cyclone Separator. A common cyclone separator generally consists of an air-inlet, a cylinder, a cone, a dust-outlet, and an exhaust pipe. After the gas which contains hazardous materials enters the cylinder in a certain speed, its linear motion becomes a rotating descending spiral

Table 1: Initial basic parameters of the combined separator.

Geometric parameters	Proportion (Relative to D)
Cylinder height H1	1
Cone height H2	1.2
Air-inlet a × b	0.2×0.3
Inner exhaust pipe diameter d	0.5
Inner exhaust pipe diameter h	0.4
Dust outlet B1	0.43
Outer exhaust pipe diameter B2	0.27
Filter cartridge diameter B3	0.33
Filter cartridge height H3	0.83

∗Normalized with cyclone diameter D=600 mm.

motion after being affected by the wall. The particles will be affected by centrifugal force and being smashed to the wall. It loses the inertial force and then falls along the wall surface after colliding with the wall surface. Finally it falls into the dust-outlet and is collected. And the airflow reaches the bottom and then rotates upwards, escaping from the exhaust pipe.

Therefore, the main features of the cyclone separator are the simple internal structure, no internal structure, high efficiency, convenient maintenance, and low manufacturing cost. It is widely used in a variety of occasions, especially in the high concentration and high temperature and pressure condition. It is mostly used to capture larger fine particles. Because of the smaller tiny particles with less centrifugal force than air resistance, they are not easily captured and will flow directly from the exhaust pipe with the inner vortex.

2.2. The Combined Cyclone and Filter Cartridge Separator. After adding a filter cartridge to the exhaust pipe of the cyclone separator, the cyclone separator's ability to handle larger particles is retained. The inner filter cartridge of the exhaust pipe can capture smaller fine particles (short-circuit flow, upper gray ring, and dust outlet back-mixed particles) that cannot be captured by the cyclone separator. This mitigates the shortcomings of the cyclone separator. Only small amounts of particles are captured by the filter cartridge because most of the hazardous material particles are captured by the cyclone separation part of the combined model. Finally, the particle stacking speed on the surface of the filter cartridge and the frequency of cleaning were reduced, and the working life of the filter cartridge was increased. The model structure is shown in Figure 2 and basic parameters are listed in Table 1.

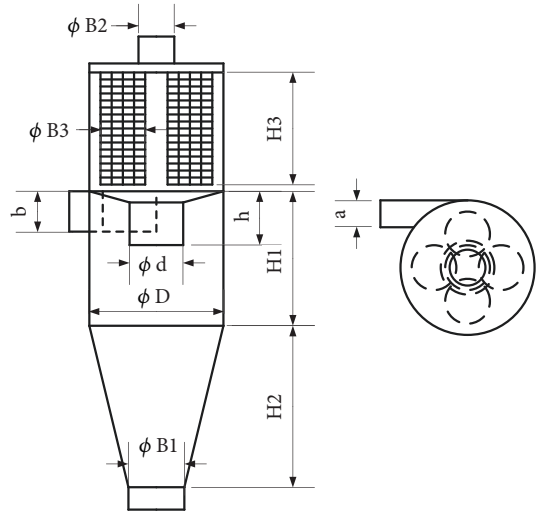

Figure 2: Diagram of combined separator structure.

2.3. The Analysis of Numerical Simulation

2.3.1. The Governing Equation of Fluid Flow

(1) The Continuous Equation of Fluid. Any flow must satisfy the law of conservation of mass. The increase in the fluid microbody body mass per unit time is equal to the net mass flowing into the microbody during the same time interval.

$$\frac{\partial \rho}{\partial t} + \frac{\partial}{\partial x_i}(\rho u_i) = 0 \tag{1}$$

where ρ is the fluid density and u is the fluid velocity.

(2) The Momentum Conservation Equation of Fluid. The momentum conservation is also the basic law of fluid flow. The momentum change rate of the fluid in the microbody is equal to the sum of the forces acting on it.

$$\begin{aligned}\frac{\partial}{\partial t}(\rho u_i) + \frac{\partial}{\partial x_j}(\rho u_i u_j) &= -\frac{\partial}{\partial x_i} + \frac{\partial}{\partial x_j}\left[u\left(\frac{\partial u_i}{\partial x_j} + \frac{\partial u_j}{\partial x_i} - \frac{2}{3}\delta_{ij}\frac{\partial u_i}{\partial x_i}\right)\right] \\ &+ \frac{\partial}{\partial x_j}\left(-\rho\overline{u_i' u_j'}\right)\end{aligned} \tag{2}$$

2.3.2. The Numerical Simulation Method. The gas-solid two-phase flow of the combined separator was numerically simulated using FLUENT software. The combined model structure is complex and the internal gas flow is a three-dimensional strong turbulent flow. To achieve an accurate reflection of the anisotropic effect in the flow field, the Reynolds Stress Model (RSM) was used in the gas phase flow field simulation [20]. This model (RSM) is suitable for high rotational flow. Moreover, the Reynolds Stress Model considers the rapid changes in streamline bending, vortex, rotation, and tension. It has a higher accuracy prediction potential for complex flows [21, 22]. RSM transport equation [23, 24] is as follows:

$$\frac{\partial\left(\rho\overline{u_i'u_j'}\right)}{\partial t}+\frac{\partial\left(\rho u_k\overline{u_i'u_j'}\right)}{\partial t} = D_{i,j}+P_{i,j}+G_{i,j}+\emptyset_{i,j}-\varepsilon_{i,j}+F_{i,j}+S_{i,j} \tag{3}$$

where

$D_{i,j}$ is the diffusion term $D_{i,j} = -(\partial/\partial x_k)[\rho\overline{u_i'u_j'u_k'} + \overline{p(\delta_{kj}u_i' + \delta_{jk}u_j')} - u(\partial/\partial x_k)\overline{(u_i'u_j')}]$

$P_{i,j}$ is the shear production term $P_{i,j} = -\rho(\overline{u_i'u_j'}(\partial u_j/\partial x_k) + \overline{u_j'u_k'}(\partial u_i/\partial x_k))$

$G_{i,j}$ is the buoyancy production term $G_{i,j} = -\rho\beta(g\overline{u_j'\theta} + g\overline{u_i'\theta})$

$\emptyset_{i,j}$ is the pressure strain redistribution term $\emptyset_{i,j} = \overline{p(\partial u_i'/\partial x_j + \partial u_j'/\partial x_i)}$

$\varepsilon_{i,j}$ is the dissipation term $\varepsilon_{i,j} = 2u\overline{(\partial u_i'/\partial x_k)(\partial u_j'/\partial x_k)}$

$F_{i,j}$ is the rotating system production term $F_{i,j} = -2\rho\gamma_k(\overline{u_j'u_m'}\varepsilon_{ikm} + \overline{u_i'u_m'}\varepsilon_{jkm})$

$S_{i,j}$ is the source term

Next, the pressure interpolation format selects the PRESTO, because PRESTO, which is very suitable for high-speed rotating flow and porous media models, can best reflect the internal flow field of the combination. The solution of pressure coupling selects the mass, momentum, and energy transfer equations of SIMPLE semi-implicit method. The QUICK difference format is used in the convection term of each equation.

2.3.3. The Discrete Phase. Because the hazardous materials collection truck collects the hazardous material particles using vacuum negative pressure, a two-phase flow with a very small particle volume fraction is collected. In the FLUENT simulation analysis, the gas belongs to the continuous phase, and the hazardous materials particles are sparse phases. Therefore, the DPM model suitable for gas-solid two-phase flow with a volume fraction of less than ten percent is applied. The DPM model [24–26] uses the Euler-Lagrangian calculation idea, where the continuous fluid phase is processed in Euler coordinates and the particle phase is processed under the Lagrangian framework. The control equation for a single particle can be derived from Newton's second law.

$$m_p\frac{d\overline{V_P}}{d_t} = \overline{F_D}+\overline{F_P}+\overline{F_A}+\overline{F_B}+\overline{F_S}+\overline{F_M}+\overline{F_G}+\overline{F_C} \tag{4}$$

where $\overline{F_D}$ is the drag force generated by the viscosity of the fluid on the particles, $\overline{F_P}$ is the pressure gradient force, an additional nonuniform force caused by the flow field pressure gradient, $\overline{F_A}$ is the additional mass force caused by the asymmetric pressure of the upper and lower surfaces after the particles are accelerated, $\overline{F_B}$ is the Basset force generated by the acceleration or deceleration of particles in a fluid, $\overline{F_S}$ is the Saffman force generated by the presence of velocity gradient in the flow field, $\overline{F_M}$ is the Magnus force generated by the rotation of the particles in the flow field, $\overline{F_G}$ is the volume force produced by gravity, and $\overline{F_C}$ is the force generated between the particles and the particles, particles and the wall. Although particles are subjected to several forces [27] in a combined model, they are not important for their own movements. Given that the gas density is much smaller than the density of the particles, the force includes buoyancy, pressure, and gradient force, and it can be negligible compared to the inertia experienced by the particles. The most important of all the above forces is the drag [23, 28], whose expression is as follows:

$$\overline{F_D} = \frac{18uC_DRe_p}{\rho_v d_v^2 24}(u-u_P)$$
$$Re_p = \frac{\rho_p d_p\left|u-u_p\right|}{u} \tag{5}$$

where C_D is the drag coefficient: $0 < Re_p \le 1$, $C_D = Re_p/24$; $Re_p > 1000$, and $C_D = 0.44$; else $C_D = (Re_p/24)(1 + 0.15Re_p^{0.687})$; R_{e_p} is the Reynolds number.

2.3.4. The Boundary Conditions. Given that the hazardous material collection truck collects hazardous materials using vacuum negative pressure (the condition at the gas outlet is 0.8 atmospheres), the overlet boundary condition is set to pressure-outlet, and the discrete phase boundary condition is set to ESCAPE in the FLUENT software. The boundary condition at the inlet is set to pressure-inlet and the discrete phase boundary condition is set to ESCAPE. In this study, it is assumed that the airflow of the dust outlet is zero, the boundary condition at the dust outlet is set to wall, and the discrete phase boundary condition is set to TRAP. The porous medium boundary condition is set to Porous-jump and the discrete phase boundary condition is set to INTERIOR. The wall is set to no-slip boundary and the roughness is set to the default roughness of 0.5. The discrete phase boundary condition of wall is set to REFLECT, and there is a complete collision between the particle and the wall.

Given the large number of geometrical pores on the surface of the filter cartridge, meshing is difficult to achieve. Therefore, the geometric pores are simplified in the geometric meshing, and the filter cartridge is treated as a cylinder. When

Table 2: Basic parameters of model simulation.

Geometric parameter	Value of number
Particle density ρ/kg·m^{-1}	2700
Permeability α/m^2	1e-8
Thickness of the porous medium n/mm	2
Air-inlet gauge total pressure P_1/atm	0.0025
Outer exhaust pipe gauge pressure P_2/atm	-0.2
Pressure jump coefficient C_2	0
Particle diameter d_k/um	1

analyzing fluids using FLUENT software, the cylindrical region is set to the porous medium fluid domain with a source of resistance. A velocity-dependent momentum is generally provided in the porous region [29], and its expression is as follows:

$$S_i = -\left(\sum_{j=1}^{3} D_{ij} u v_j + \sum_{j=1}^{3} C_{ij} \frac{1}{2} \rho |v| v_j\right) \tag{6}$$

where the first item on the right side of the expression is the viscous-loss term and the second item is the inertia-loss term. For porous media, it can be changed to another expression:

$$S_i = -\left(\frac{u}{\alpha} v_i + C_2 \frac{1}{2} |v| v_i\right) \tag{7}$$

where α is the permeability and C_2 is the pressure jump coefficient. Here, the matrix D is $1/\alpha$. Momentum acts on the fluid to create a pressure gradient, $\nabla p = S_i$, which can be written as $\nabla P = -S_i n$. In the expression, n is the thickness of the porous medium domain. The permeability value and pressure jump coefficient are determined according to Reference [30] and the actual conditions. The parameters of filter cartridge type dust collector are listed in Table 2.

3. The Response Surface Method Parameter Design and Numerical Simulation Results

3.1. The Response Surface Methodology and Parameter Design. The response surface methodology is a structural parameter optimization method, which is a combination of mathematical methods and statistical methods. It was first proposed by Box and Wilson [31] in 1951. The response surface methodology is a method of creating a surface by determining the real value of a function of many points around one point. In an area that is close enough to this point, this surface is used instead of this actual model to operate. To facilitate the analysis and find the optimal value of the variable, the surface response function replaces the complex model with a higher order function relationship. The basic steps of the response surface method analysis in this study are as follows: First, the least squares method is used to estimate the coefficient of the surface response function. Then, the response equation is obtained. Finally, the degree of influence of each factor on the target is obtained, through the method of significant examination analysis. The second-order design is chosen in this study, and the expression of the response function [11, 32] is as follows:

$$y = \beta_0 + \sum_{i=1}^{k} \beta_i x_i + \sum_{i=1}^{k} \beta_{ii} x_i^2 + \sum_{i<1}^{k} \beta_{ij} x_i x_j + \varepsilon \tag{8}$$

where β_0, β_i, β_{ii}, and β_{ij} represent the regression coefficients of primary, secondary, and interaction, respectively, x is an independent variable, y is the objective function, k is the number of influencing factors, and ε is the error of the objective function. This second-order polynomial can replace the real function within a certain range.

Because of the existence of the filter cartridge in the combined model, the filtration rate for 1-μm hazardous materials particles can reach 99.9%. However, too much reliance on the filter cartridge to capture the particles will cause the combined model to lose its meaning. The particles are separated as far as possible by the rotating separation structure, and finally the tiny particles that cannot be separated are captured by the filter cartridge. Such a method can reduce the workload of the filter cartridge, reducing the accumulation speed of particles on the surface of the filter cartridge, reducing the frequency of cleaning. Therefore, the separation efficiency of the cyclone separation structure is used as a response function.

In this study, the influence factors of the inner exhaust pipe diameter d, inner exhaust pipe insertion depth h, cylinder height H1, and cone height H2 are selected as the optimization parameters. The diameter D of the cylinder is taken as a fixed value. According to the conventional cyclone separator optimization [32–34] and the size of the filter cartridge and then referring to the size of the hazardous materials rescue truck, the cylinder diameter is set to D=600 mm, and the variation range of the independent variable is as listed in Table 3.

The Box-Behnken second-order design method of response surface methodology was used to optimize the structure in this study. There are $3^4 = 81$ different structures of combined separators for four factors and three levels of optimization variables. After using the BBD design method for calculation, the number of experimental groups was 29, which includes the center experiment 5 times. The design table created by Box-Behnken is listed in Table 4.

3.2. Simulation Results. The combined model is divided into structured hexahedral meshes using ICEM software, and the

Table 3: Ratio change range of optimization parameter.

Optimized variable	Initial proportion	Proportion of change range
Inner exhaust pipe diameter d/D	0.5	0.4~0.6
Inner exhaust pipe insertion depth h/D	0.4	0.2~0.6
Cylinder height H1/D	1	0.8~1.2
Cone height H2/D	1.2	1~1.4

Table 4: Parameters table.

Level	X1 (inner exhaust pipe diameter d/mm)	X2 (inner exhaust pipe insertion depth h/mm)	X3 (cylinder height H1/mm)	X4 (cone height H2/mm)
−1	240	120	480	600
0	300	240	600	720
1	360	360	720	840

mesh is imported into FLUENT software. Then, we can obtain simulation results of 29 different structural models. Here is an example of the seventh group of simulation results. The model mesh is shown in Figure 3(a), and the simulated contour figure is shown in Figures 3(b), 3(c), and 3(d).

It can be seen from the speed contour figure of model in Figure 3(b) that the speed increases and then decreases from the wall surface of the combined model to the center. There is maximum speed at the position of inner exhaust pipe and minimum speed at the center of the combined model. Figure 3(c) is the trajectory tracking of particles exhaust pipe, and the particle trajectory is rotating. Some of the particles are separated by rotation, and only a small part of the particles will escape to the surface of the filter cartridge and will eventually be captured. Figure 3(d) shows the dynamic pressure contour figure at y=−240, and the dynamic pressure is symmetrically distributed.

4. Analysis and Optimization

4.1. Regression Analysis. After the combined models of different sizes are imported into the FLUENT software individually to simulate and the filter cartridge boundary condition is set to Porous-jump, the discrete phase is set to TRAP when capturing particles, and the particle capture rate of each model, which denotes the ability of the filter cartridge and the cyclone separation structure to work together, is 99.9%. When the discrete phase at the filter cartridge is set to INTERIOR and the discrete phase of the dust outlet is set to TRAP, the separation efficiency is between 0% and 99.9%. Such a method can obtain the separation efficiency y of the combined model cyclone separation structure. Then, the simulated separation efficiency y is imported into the Design-Expert software, and the result is fitted by the least squares method. Table 5 presents the variance analysis of the quadratic equation, and Table 6 presents the fit statistics.

The judging criteria are as follows:

(1) The model significance check P value: usually $P \leq 0.05$ indicates that the model is considered very significant or a factor has a significant impact on the model

(2) The determination coefficient R^2: in engineering applications, $R^2 > 0.8$ is considered to be approximately credible, and $R^2 > 0.95$ is relatively high

(3) The closer the correction coefficient R^2 (adjusted R^2) and the prediction coefficient R^2 (predicted R^2), the better

(4) Signal-to-noise ratio: this indicates the resistance of the fitting function to bad data interference (Adeq precision). If the value is higher than 4 in engineering applications, then the fitting degree is better

It can be seen from Table 5 that some P values are much less than 0.05, which indicates that these factors have a significant impact on the model. The P value of the model is less than 0.0001, which indicates that the second-order equation fits well. From Table 6, it is seen that the fitness R2 = 0.9657; the correction factor and the prediction coefficient are very close, and the signal-to-noise ratio is much larger than 4. These phenomena indicate that the second-order equation fits well.

In the process of establishing a regression model, owing to the designer's mistakes or accidental factors, the data we get is often not completely reliable (data anomaly). Sometimes, this does not rule out the above problems in the data, even if the P value in the results proves that the regression equation is reliable. The purpose of residual analysis is to address this issue. The residual indicates the difference between the actual observed value and the estimated value (fitted value). Figure 4(a) is the residual normal probability distribution figure. Figure 4(b) is the relationship between experimental values and predicted values. It can be seen from the figure that the predicted value and the actual value are roughly distributed on a straight line, and each scatter point in the residual figure has a linear trend. This phenomenon indicates that the response value of the model can roughly reflect the actual value of the model. The residuals are in a normal distribution, and the model has a good fit. Figure 4(c) shows the relationship between the residual and the predicted value of the equation. The points on the graph are scattered irregularly, and the effect is better. Most of the points are in the horizontal band zone, and there is no random distribution

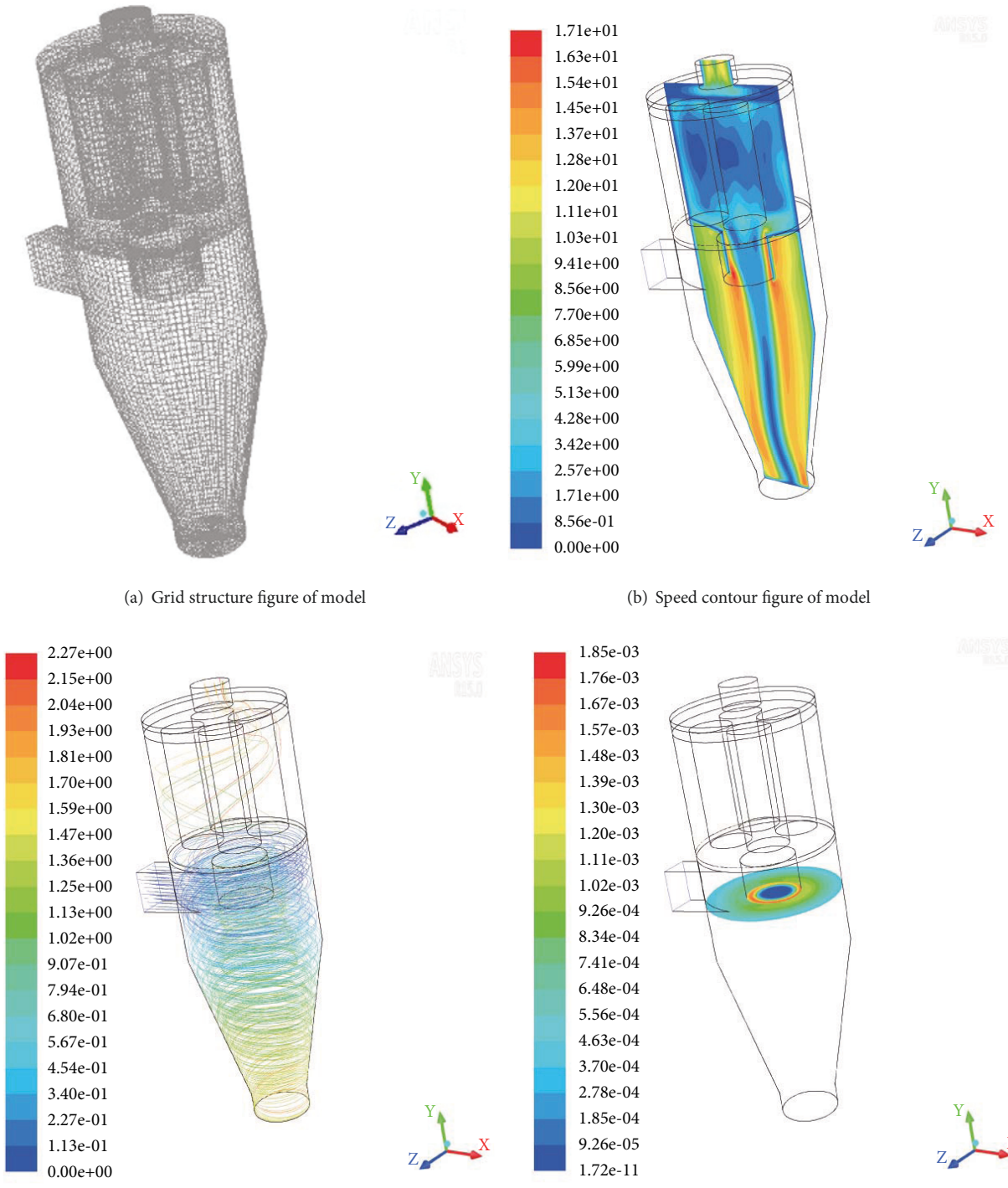

(a) Grid structure figure of model

(b) Speed contour figure of model

(c) Trajectory tracking of particles

(d) Dynamic pressure contour figure at y=−240

Figure 3: Grid and simulation contour figure of combined mode.

of any systematic trend, which indicates that the regression equation fits the sample data well.

Figure 5 shows the effect of various factors on separation efficiency. As seen from Figure 5(a), the separation efficiency decreases continuously when the diameter d of the inner exhaust pipe increases continuously. Because the external rotating fluid region decreases and the internal rotating fluid region increases when the diameter of the exhaust pipe increases, the particles will be easily caught by the internal swirling flow into the inner exhaust pipe, resulting in a decrease in separation efficiency after the particles escape. Comparing Figures 5(a) and 5(b), when the inner exhaust

Table 5: ANOVA for the quadratic model.

Source	Sum of Squares	df	Mean Square	F-value	p-value	
Model	3753.82	14	268.43	28.13	<0.0001	significant
A-X1	1722.01	1	1722.01	180.63	<0.0001	
B-X2	325.52	1	325.52	34.15	<0.0001	
C-X3	325.52	1	325.52	34.15	<0.0001	
D-X4	1031.38	1	1031.38	108.19	<0.0001	
AB	189.06	1	189.06	19.83	0.0005	
AC	0.3906	1	0.3906	0.0410	0.8425	
AD	0.0000	1	0.0000	0.0000	1.0000	
BC	76.56	1	76.56	8.03	0.0133	
BD	25.00	1	25.00	2.62	0.1277	
CD	0.3906	1	0.3906	0.0410	0.8425	
A2	19.16	1	19.16	2.01	0.1781	
B2	31.04	1	31.04	3.26	0.0927	
C2	0.6334	1	0.6334	0.6334	0.8003	
D2	26.76	1	26.76	2.81	0.1160	
Residual	133.46	14	9.53			
Lack of Fit	133.46	10	13.35			
Pure Error	0.0000	4	0.0000			
Cor Total	3887.28	28				

Table 6: Fit statistics.

Regression Coefficient	Value	Regression Coefficient	Value
Std. Dev	3.09	Adjusted R^2	0.9313
Mean	56.16	Predicted R^2	0.8022
C.V.%	5.50	Adeq Precision	20.4762
R^2	0.9657		

pipe diameter d is larger, the separation efficiency decreases by a large margin after the inner exhaust pipe insertion depth h is decreased. This phenomenon indicates that the interaction between the inner exhaust pipe diameter and the inner exhaust pipe insertion depth has a significant effect on the separation efficiency. As seen from Figure 5(c), the separation efficiency decreases as the height H1 of the cylinder and the height H2 of the cone decrease. This phenomenon may be caused by the decrease in the rotational strength of the wake vortex when the height of the combined model is increased. Then, the particles are not easily taken away, and the separation efficiency is reduced after the particles escape.

After taking the center experimental group X1, X2, X3, and X4=300 mm, 240 mm, 600 mm, and 720 mm, respectively, and keeping three of the factors unchanged, the influence of each factor shown in Figure 6 on the separation efficiency can be obtained when the remaining factor is changed. From Figures 6(a), 6(c), and 6(d), we can find that the separation efficiency will increase or decrease monotonically. In addition, the relatively large slope of the inner exhaust pipe diameter and the cone height indicates that the separation effect is considerably affected. However, we can find from Figure 6(b) that when the depth of the inner exhaust pipe is increased to a certain depth, the separation efficiency will not increase any more. This phenomenon can also be seen from Figure 5(a). It can be analyzed that when the insertion depth of the inner exhaust pipe is low, the particles easily escape from the inner exhaust pipe in the form of a short-circuit flow. However, when the depth of the inner exhaust pipe is too high, the particles will be collected on the wall above the inner exhaust pipe to form an "ash ring," which is not easily discharged or captured. This will cause difficulties in the particles getting discharged or captured; however, the phenomenon that the inclination rate shown in Figure 5(d) is gradually decreased indicates that the magnitude of increase of separation efficiency is decreased. After the height of the cylinder and the cone is increased to a certain extent, a larger negative pressure may be required to maintain the effective separation of the particles under the boundary conditions of the vacuum negative pressure.

4.2. Structural Optimization. The model fits well in this study, but there are nonsignificant items. Therefore, the cross-terms with less influence on the fitting function are removed. Then, the coefficients in terms of coded factors are obtained, which are listed in Table 7.

The coefficient estimate represents the expected change in response per unit change in factor value when all remaining factors are held constant. The intercept in an orthogonal design is the overall average response of all the runs. The

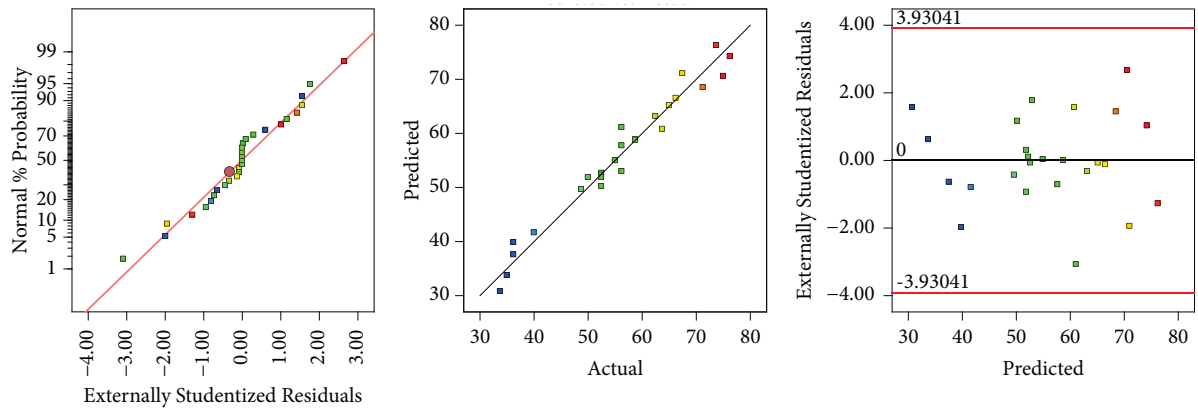

(a) Normal plot of residuals (b) Predicted vs. actual (c) Residuals vs. predicted

Figure 4: Data diagnostics.

Table 7: Coefficients in terms of coded factors.

Factor	Coefficient Estimate	Standard Error	95% CI Low	95% CI High	VIF
Intercept	58.55	1.01	56.43	60.66	
A-X1	−11.98	0.7902	−13.64	−10.32	1.0000
B-X2	5.21	0.7902	3.55	6.87	1.0000
C-X3	5.21	0.7902	3.55	6.87	1.0000
D-X4	9.27	0.7902	7.61	10.93	1.0000
AB	6.88	1.37	4.00	9.75	1.0000
BC	4.38	1.37	1.50	7.25	1.0000
BD	−2.50	1.37	−5.38	0.3755	1.0000
A^2	−1.66	1.06	−3.88	0.5577	1.05
B^2	−2.13	1.06	−4.35	0.0889	1.05
C^2	−1.97	1.06	−4.19	0.2452	1.05

coefficients are adjustments around that average based on the factor settings. When the factors are orthogonal, the VIFs are 1; VIFs higher than 1 indicate multicollinearity, and the higher the VIF, the more severe the correlation of factors. As a rough rule, VIFs less than 10 are tolerable.

Through the coefficients in terms of coded factors in Table 7, we can get the regression equation of the actual separation efficiency as follows:

$$\begin{aligned} y = {} & -12.14105 - 0.152215 * X_1 - 0.229401 * X_2 \\ & - 0.029514 * X_3 + 0.316136 * X_4 + 0.000955 \\ & * X_1 * X_2 + 0.000304 X_2 * X_3 - 0.000174 X_2 \\ & * X_4 - 0.000461 * X1^2 - 0.000148 * X2^2 \\ & - 0.000137 * X4^2 \end{aligned} \quad (9)$$

In this study, the combined model is optimized to reduce the workload of the filter cartridge as much as possible, so it is necessary to increase the particle capture rate of the combined model cyclone separation structure. Therefore, the combined model is optimized within the optimization interval. The optimization interval and the optimum point are listed in Table 8.

After performing CFD simulation on the optimized structural dimensions listed in Table 8, the separation efficiency of the cyclone separation structure can be obtained. It can be seen from Table 9 that the predicted separation efficiency value y_R obtained by the response surface methodology (RSM) design test is very close to the result y obtained by the CFD simulation. This result shows that the response surface methodology (RSM) of Design-Expert software can well predict the separation performance of different structural sizes of the combined model.

5. Conclusion

In this study, most of the external structure of the cyclone separator is retained for the combined model. The method of adding the filter cartridge above the combined model can capture the particles well, and the total capture rate of the particles can reach 99.9%. It can be seen from the simulation results that this method not only utilizes the characteristics of the original cyclone but also utilizes the filter cartridge to capture the characteristics of tiny particles. This method reduces the probability of particles escaping from the exhaust port towing to dust outlet back-mixing, short-circuit flow, and upper gray ring. Applying this highly

Table 8: Optimization constraints and results.

Name	Goal	Lower Limit	Upper Limit	Optimization Results
A: X_1 (mm)	is in range	240	360	240.000
B: X_2 (mm)	is in range	120	360	244.342
C: X_3 (mm)	is in range	480	720	720.000
D: X_4 (mm)	is in range	600	840	840.000
y (%)	maximize	0	100	81.379

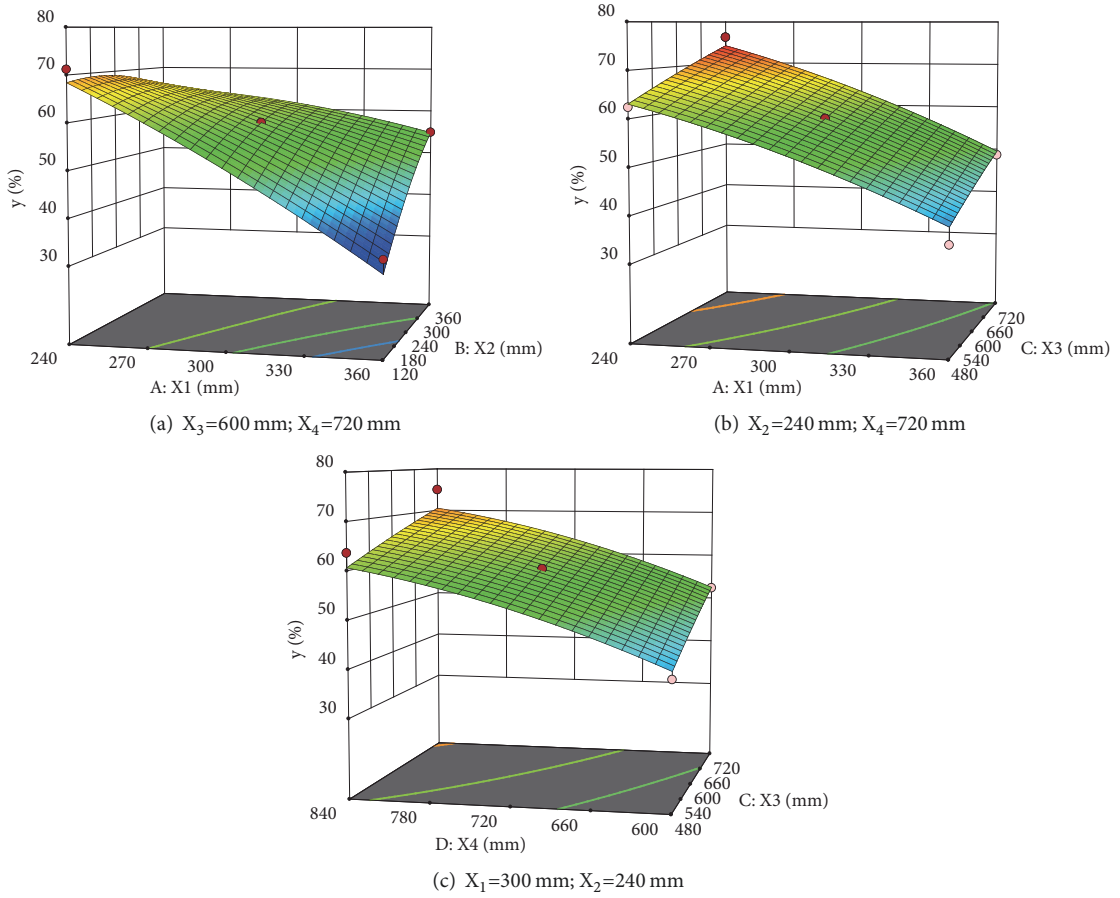

(a) X_3=600 mm; X_4=720 mm

(b) X_2=240 mm; X_4=720 mm

(c) X_1=300 mm; X_2=240 mm

Figure 5: Effect of different factors on separation efficiency.

Table 9: Model prediction values and numerical simulation values.

	Response Surface Methodology	CFD Simulation	Error
y	81.379%	81.25%	0.129%

efficient combined model to separate hazardous material will reduce the probability of secondary pollution.

After structural optimization of the combined model by applying response surface methodology, we can see that the most important influence on the separation effect of the cyclone separation part is the inner exhaust pipe diameter and cone height. The insertion depth of the inner exhaust pipe and the height of the cylinder also have an effect on the separation efficiency, but their effect is small. The interaction between the diameter and insertion depth of the inner exhaust pipe has an effect on the separation efficiency. After the insertion depth of the inner exhaust pipe is increased, the separation efficiency is increased to no change, and there is an optimum value of the insertion depth here. Furthermore, the effect of the other three factors on the separation efficiency is monotonic, but the magnitude of increase of separation efficiency is decreased after the total height of the cone and cyclone increases.

Among the 29 data values, the poorest cyclone separation structure separation efficiency is 35%, and the workload of the filter cartridge is nearly twice that of the cyclone separation structure. The combined model optimized in a reasonable interval is introduced into the CFD simulation, and the predicted value of the separation efficiency model of the cyclone separation structure is different from the CFD

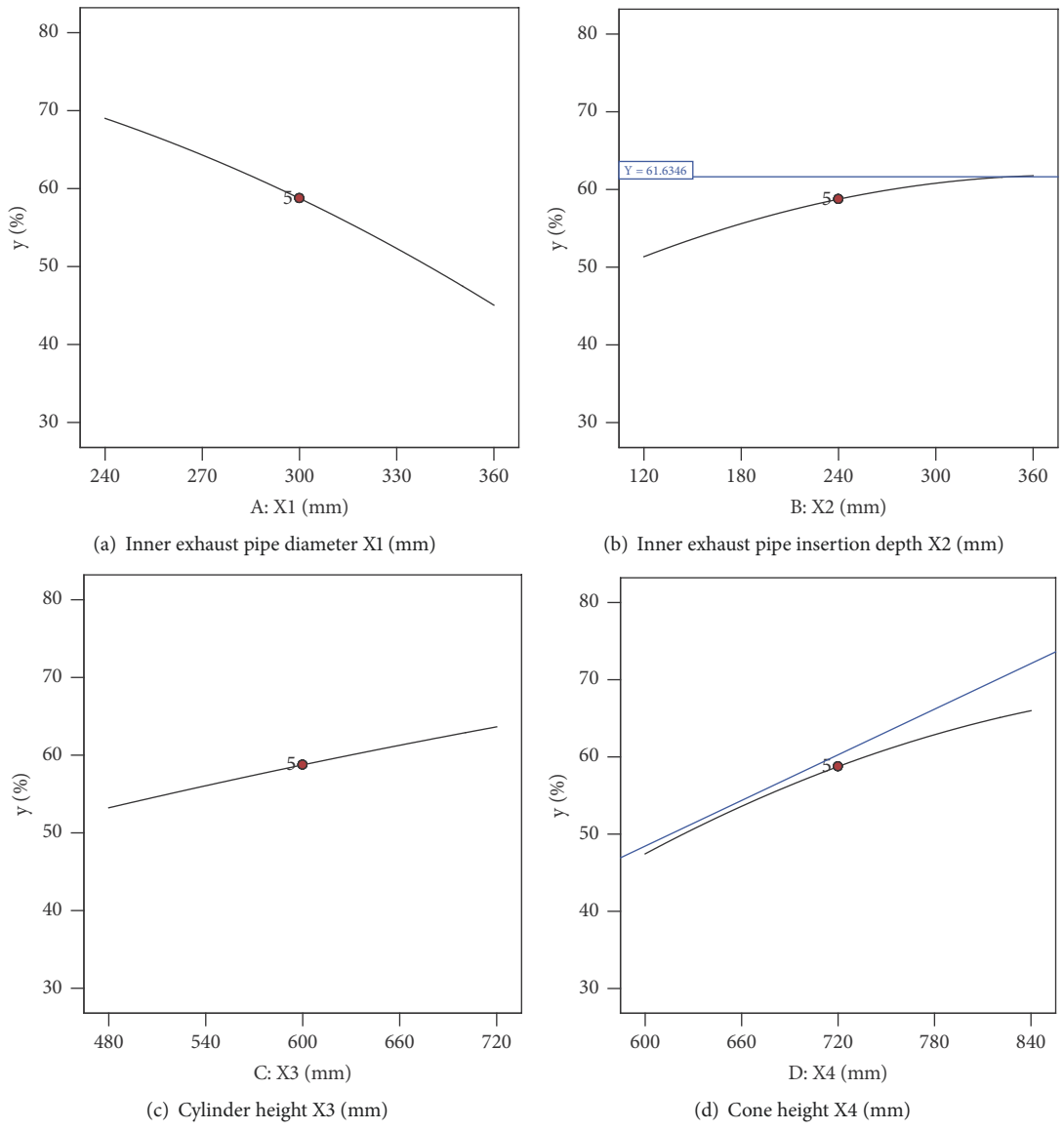

(a) Inner exhaust pipe diameter X1 (mm)

(b) Inner exhaust pipe insertion depth X2 (mm)

(c) Cylinder height X3 (mm)

(d) Cone height X4 (mm)

Figure 6: Effect of a single factor on efficiency.

simulation value by 0.129%. This result indicates that this experimental design is a good predictor of the separation performance of the combined model. After optimization, 81.25% of the 1-μm particles can be removed by the cyclone separation part, and only 18.75% are removed by the filter cartridge. This combined model considerably reduces the workload of the filter cartridge, thereby reducing the stacking speed of the particles on the surface of the filter cartridge and increasing the working life of the filter cartridge.

Data Availability

No data were used to support this study.

Conflicts of Interest

The authors declare no conflicts of interest.

Acknowledgments

The authors would like to acknowledge the project supported by National Key R&D Program of China (No. 2017YFC0804805).

References

[1] A. Hoffmann, L. Stein, and P. Bradshaw, "Gas cyclones and swirl tubes: principles, design and operation," *Applied Mechanics Reviews*, vol. 56, no. 2, p. B28, 2003.

[2] C. J. Stairmand, "The design and performance of cyclone separators," *Transactions of the Institution of Chemical Engineers*, vol. 29, pp. 356–383, 1951.

[3] W. Barth, "Design and layout of the cyclone separator on the basis of new investigations," *Brennstoff Wärme Kraft*, vol. 8, no. 1, pp. 1–9, 1956.

[4] I. Karagoz and A. Avci, "Modelling of the pressure drop in tangential inlet cyclone separators," *Aerosol Science and Technology*, vol. 39, no. 9, pp. 857–865, 2005.

[5] J. Casal and J. M. Martinez-Benet, "A better way to calculate cyclone pressure drop," *Chemical Engineering*, vol. 90, no. 2, pp. 99-100, 1983.

[6] J. Dirgo, *Relationship between cyclone dimensions and performance [Ph.D. thesis]*, Harvard University, USA, 1988.

[7] G. Ramachandran, D. Leith, J. Dirgo, and H. Feldman, "Cyclone optimization based on a new empirical model for pressure drop," *Aerosol Science and Technology*, vol. 15, no. 2, pp. 135–148, 1991.

[8] W. D. Griffiths and F. Boysan, "Computational fluid dynamics (CFD) and empirical modelling of the performance of a number of cyclone samplers," *Journal of Aerosol Science*, vol. 27, no. 2, pp. 281–304, 1996.

[9] J. Gimbun, T. G. Chuah, A. Fakhru'l-Razi, and T. S. Y. Choong, "The influence of temperature and inlet velocity on cyclone pressure drop: a CFD study," *Chemical Engineering and Processing: Process Intensification*, vol. 44, no. 1, pp. 7–12, 2005.

[10] M. Azadi, M. Azadi, and A. Mohebbi, "A CFD study of the effect of cyclone size on its performance parameters," *Journal of Hazardous Materials*, vol. 182, no. 1-3, pp. 835–841, 2010.

[11] K. Elsayed Khairy and C. Lacor, "Optimization of the cyclone separator geometry for minimum pressure drop using mathematical models and CFD simulations," *Chemical Engineering Science*, vol. 65, no. 22, pp. 6048–6058, 2010.

[12] P. K. Swamee, N. Aggarwal, and K. Bhobhiya, "Optimum design of cyclone separator," *AIChE Journal*, vol. 55, no. 9, pp. 2279–2283, 2009.

[13] J. Tu, G. H. Yeoh, and C. Liu, *Computational Fluid Dynamics: A Practical Approach*, Butterworth-Heinemann, 2018.

[14] G. Ramachandran and D. Leith, "Cyclone optimization based on a new empirical model for pressure drop," *Aerosol Science and Technology*, vol. 15, no. 2, pp. 135–148, 1991.

[15] R. D. Luciano, B. L. Silva, L. M. Rosa, and H. F. Meier, "Multi-objective optimization of cyclone separators in series based on computational fluid dynamics," *Powder Technology*, vol. 325, pp. 452–466, 2018.

[16] O. L. Sgrott, D. Noriler, V. R. Wiggers, and H. F. Meier, "Cyclone optimization by COMPLEX method and CFD simulation," *Powder Technology*, vol. 277, pp. 11–21, 2015.

[17] G. Ravi, S. K. Gupta, and M. B. Ray, "Multi-objective optimization of cyclone separators using genetic algorithm," *Industrial & Engineering Chemistry Research*, vol. 39, no. 11, pp. 4272–4286, 2000.

[18] Y. Z. Zhang, H. Y. Chen, and J. Z. Tan, "Filter cartridge type dust collector and its application status," *Energy and Environment*, no. 5, pp. 47–49, 2009.

[19] Y. J. Sun, Y. L. Ou, and C. Z. Yang, "Filter cartridge type dust collector and its application," *Ventilation and Dust Removal*, no. 2, pp. 26–28, 1995.

[20] S. Y. Liu, Y. Zhang, and B. G. Wang, "Simulation of three-dimensional turbulent flow field in a cyclone with RSM," *Transactions of Beijing Institute of Technology*, vol. 25, no. 5, pp. 378–383, 2005.

[21] K. Pant, C. T. Crowe, and P. Irving, "On the design of miniature cyclones for the collection of bioaerosols," *Powder Technology*, vol. 125, no. 2-3, pp. 260–265, 2002.

[22] G. Jolius, T. G. Chuah, A. Fakhru'l-Razi et al., "The influence of temperature and inlet velocity on cyclone pressure drop: a CFD study," *Chemical Engineering and Processing: Process Intensification*, vol. 44, no. 1, pp. 7–12, 2005.

[23] B. Wang, D. L. Xu, K. W. Chu, and A. B. Yu, "Numerical study of gas-solid flow in a cyclone separator," *Applied Mathematical Modelling*, vol. 30, no. 11, pp. 1326–1342, 2006.

[24] T. Zhou, *Gas-Solid Two-Phase Characteristics Study and Numerical Simulation of Cyclone Separator*, Shanghai Jiao Tong University Press, Shanghai, China, 2007.

[25] Z. L. Yuan, L. P. Zhu, and F. Geng, *Gas-Solid Two-Phase Flow and Numerical Simulation*, Southeast University Press, Jiangsu, China, 2013.

[26] H. Safikhani, M. A. Akhavan-Behabadi, M. Shams, and M. H. Rahimyan, "Numerical simulation of flow field in three types of standard cyclone separators," *Advanced Powder Technology*, vol. 21, no. 4, pp. 435–442, 2010.

[27] K. F. Cen, M. J. Ni, and J. H. Yan, *Gas-Solid Separation Theory and Technology*, Zhejiang University Press, Zhejiang, China, 1999.

[28] B. Zhao, Y. Su, and J. Zhang, "Simulation of gas flow pattern and separation efficiency in cyclone with conventional single and spiral double inlet configuration," *Chemical Engineering Research and Design*, vol. 84, no. 12, pp. 1158–1165, 2006.

[29] K. Hu, Z. H. Gu, and H. F. Ma, *ANSYS CFD Detailed Examples of Difficult Problems*, Post and Telecom Press, Beijing, China, 2017.

[30] Z. M. Gu, L. J. Guo, and H. Gao, "Numerical simulation and analysis of gas-Solid two-Phase flow in a submerged filter cartridge dust collector," *Chemical Engineering & Machinery*, vol. 29, no. 4, pp. 197–202, 2002.

[31] G. E. Box and K. B. Wilson, "On the experimental attainment of optimum conditions," *Journal of the Royal Statistical Society: Series B (Methodological)*, vol. 13, no. 1, pp. 1–38, 1951.

[32] K. Elsayed and C. Lacor, "CFD modeling and multi-objective optimization of cyclone geometry using desirability function, artificial neural networks and genetic algorithms," *Applied Mathematical Modelling*, vol. 37, no. 8, pp. 5680–5704, 2013.

[33] H. Safikhani, M. A. Akhavan-Behabadi, N. Nariman-Zadeh, and M. J. Mahmood Abadi, "Modeling and multi-objective optimization of square cyclones using CFD and neural networks," *Chemical Engineering Research and Design*, vol. 89, no. 3, pp. 301–309, 2011.

[34] H. Safikhani, A. Hajiloo, and M. A. Ranjbar, "Modeling and multi-objective optimization of cyclone separators using CFD and genetic algorithms," *Computers & Chemical Engineering*, vol. 35, no. 6, pp. 1064–1071, 2011.